

Article

Quantitative Analysis of Asbestos-Containing Materials Using Various Test Methods

Kiho Yang ¹, Kyu-Cheul Yoo ² and Jaewoo Jung ^{2,*}

¹ Department of Oceanography, Pusan National University, Busan 46241, Korea; kyang@pusan.ac.kr

² Division of Polar Paleoenvironment, Korea Polar Research Institute, Incheon 406840, Korea; kcyoo@kopri.re.kr

* Correspondence: jaewoo@kopri.re.kr; Tel.: +82-10-9985-1471

Received: 29 May 2020; Accepted: 23 June 2020; Published: 24 June 2020



Abstract: The advantages of X-ray powder diffraction (XRPD) analysis are its non-destructive nature, reliability, fast and easy sample preparation, and low costs. XRPD analysis has been used for mineral identification and the quantitative/qualitative determination of various types of fibrous minerals in asbestos-containing materials (ACMs). In order to test the detection limit of ACMs by XRPD, standard samples with various concentrations of ACMs (0.1%, 1%, and 3%) were fabricated using three matrix materials (talc, vermiculite, and sepiolite). Asbestiform tremolite and chrysotile were identified in the XRPD profiles of the samples with 1% and 3% ACMs. Their integral intensities were positively correlated with the concentrations. However, the XRPD peak of asbestos was not found in the samples with 0.1% ACMs. Therefore, scanning and transmission electron microscopy were utilized to investigate the samples with a very low concentration of ACMs. Although the ACM concentration (0.1%) was negligible and its direct observation was time-consuming, electron microscopy allowed for the detection of asbestos in several matrix materials. Thus, a combination of XRPD and electron microscopy improve analytical performance and data reliability.

Keywords: asbestos; elongate mineral particles; quantitative analysis; mineral identification; powder X-ray diffraction; scanning electron microscopy; transmission electron microscopy

1. Introduction

Fibrous materials have been an important part of global industries over the last several decades [1]. Asbestos is an industrial term that covers six minerals: chrysotile, crocidolite, amosite, asbestiform anthophyllite, asbestiform actinolite, and asbestiform tremolite [2–5]. It has several advantages over man-made materials, such as its mechanical strength, resistance to heat and chemicals, durability, and sound absorption effects [6,7]. Asbestos minerals can be classified into two groups: serpentine and amphibole [8,9]. Chrysotile is the most common fibrous serpentine and constitutes over 90% of asbestos used globally [1]. Asbestos amphiboles are less important industrially [10]. Asbestos and elongate mineral particles can cause asbestosis, pleural abnormalities, bronchogenic carcinomas, and mesothelioma [11–13]. Symptoms do not appear within a short period of time with the incubation period being 25 to 40 years for pulmonary asbestosis and 15 to 30 years for lung cancer, depending on the intake of asbestos [14,15]. According to a previous study, nano-size airborne particles with a mean diameter of less than 100 nm are much more toxic than expected and can cause serious health problems, including chronic bronchitis, asthma complications, respiratory tract infections, and stroke [13,15–17]. As a result, asbestos-containing materials (ACMs), used for fireproofing, insulation, construction, and friction, have been banned in 52 countries, including the United States and the European Union [18]. Multiple techniques (X-ray powder diffraction (XRPD), scanning electron microscopy (SEM) and transmission electron microscopy (TEM), Fourier transform infrared (FTIR), and Raman spectroscopy)

have been applied to detect and characterize the microparticles and nanoparticles of asbestos [7,19–23]. Until recently, the most common methods used have been electron microscopy and XRPD [24]. The most accurate method to detect asbestos has been determined to be the collection of ACMs and their microscopic examination [25]. SEM and TEM are direct observation methods and provide information on the surface features, size, shape, chemical composition, valence states, and structure of particles [26]. However, these methods are time-intensive, expensive, and destructive [27]. Moreover, it is necessary to analyze several hundreds of particles in order to guarantee that the analyzed sample is representative of the bulk sample [24]. On the contrary, XRPD analysis is fast, inexpensive, non-destructive, and reliable. Due to these advantages, XRPD has been used for mineral identification and the quantitative determination of various types of fibrous minerals in ACMs [20]. Herein, we investigate standard samples with various concentrations of ACMs (0.1%, 1%, and 3%), consisting of three matrix materials, namely talc, vermiculite, and sepiolite. These powders were prepared to compare XRPD, SEM, and TEM measurements for the quantitative determination of asbestiform tremolite with different concentrations. We also compare the results for the detection limit of asbestos (i.e., chrysotile and tremolite) in ACMs by XRPD, SEM-EDS, and TEM-EDS. We suggest that a combination of X-ray techniques and electron microscopy will improve the analytical performance and data reliability of ACM evaluation.

2. Materials and Methods

2.1. Materials

Three types of standard samples (talc (T), vermiculite (V), and sepiolite (S) matrix) containing 1% (T1–8, V1–8, and S1–8) and 3% (T9–16, V9–16, and S9–16) ACMs (i.e., chrysotile and asbestiform tremolite) were obtained from the National Institute of Environmental Research (NIER), South Korea. Additionally, talc ($\text{Mg}_3\text{Si}_4\text{O}_{11}\cdot\text{H}_2\text{O}$), vermiculite ($(\text{Mg}, \text{Al}, \text{Fe}^{2+})_3(\text{Si}, \text{Al})_4\text{O}_{10}(\text{OH})_2\cdot n\text{H}_2\text{O}$), and sepiolite ($\text{Mg}_2\text{Si}_3\text{O}_8\cdot 2\text{H}_2\text{O}$) were purchased from Sigma-Aldrich. Talc, vermiculite, and sepiolite were used to make the 0.1% asbestos standard samples used as matrix materials. Powder samples were prepared using a milling device (Planetary Mill Pulverisette-5) at NIER for the production of homogeneous ACMs. The planetary ball mill was operated at a speed of 400 rpm for 10 min.

2.2. X-ray Diffractometer

The mineralogy of the standard matrix samples (i.e., talc, vermiculite, and sepiolite) containing 0.1%, 1%, 3%, and 0% of the pure matrix (control sample) was determined using a Rigaku HR-XRD SmartLab with Cu-K α radiation (20 kV and 10 mA) at Yonsei University. Randomly oriented powder samples were homogenized with a pulverizer and by taping gently onto an automatic sample changer. The XRPD measurements were repeated five times to evaluate the homogeneity of each specimen and achieve reliable results. The XRPD profiles for a 2θ range from 3 to 60° were recorded at a scan speed of 1.5°/min, step size of 0.02°, a receiving slit size of 0.3 mm, and a divergence slit size of 1.25°. Crystallographica Search-Match software (version 2.0.3.1) was used to determine whether the prominent peaks of asbestos (i.e., chrysotile and asbestiform tremolite) could be detected, depending on the difference in content.

2.3. Scanning and Transmission Electron Microscopy (SEM and TEM)

The morphology and aspect ratio (length:width \geq 3:1) of asbestos [28,29] in the specimens were confirmed using secondary electron images with magnification in the range of $\times 200$ – $\times 1000$. The images were taken at Yonsei University with a JEOL-7800F scanning electron microscope (SEM) equipped with an energy dispersive spectrometer (EDS) operating at 15 keV and with a working distance of 6 to 10 mm. The SEM samples were prepared in such a way that the powder samples with 0.1% asbestos were attached to a sticky carbon tape. The elemental composition of the asbestos particles was measured by EDS. Transmission electron microscopy (TEM) was used to confirm the aspect ratio

(length:width) and morphology of asbestos in the specimens with 0.1% asbestos. In these samples, asbestos was not detected using only the bulk XRPD analysis. Asbestos structure and its elemental composition were acquired at the Korea Basic Science Institute, Seoul, Korea, utilizing a TECHNICAL G2 F30 field emission TEM (FE-TEM) (FEI Company, Hillsboro, OR, USA) equipped with an EDS operating at 300 kV. The 0.1% homogenized powder samples were dispersed in ethanol (0.0001 mg/mL), immersed in an ultrasonic water bath for 5 min, removed with a TEM micro Cu-grid and completely dried on a clean bench. The chemical composition of asbestos minerals was measured by EDS with an acquisition time of 30 s under the scanning transmission electron microscope (STEM) mode to confirm that the observed mineral particles were not the matrix minerals but asbestos.

2.4. Homogeneity Evaluation

In order to achieve reliable results in the process of analyzing three types of standard matrix minerals (i.e., talc, vermiculite, and sepiolite) and asbestos (i.e., chrysotile and asbestiform tremolite) mixture samples, it was essential to evaluate the homogeneity of each sample. As such, a total of 144 mixture samples (3 types of matrix \times triplet test \times 16 repetitions) were evaluated for homogeneity. One-way analysis of variance (one-way ANOVA) is a widely used statistical technique to compare group means [30]. This statistical method was applied to confirm the similarity of the proportional means of 10 different mixture powder samples. For the homogeneity assessment, the statistical values of 10 samples were evaluated at a 95% confidence level using the p-value, while the F-value was to be less than the F-rejection value [31].

3. Results and Discussion

3.1. XRPD Analysis and Homogeneity Evaluation

The XRPD analyses of talc, vermiculite, and sepiolite with different asbestos concentrations of 0.1%, 1% and 3% were compared with those of the standard materials for the quantitative analysis of asbestiform tremolite in the homogeneous materials (Figure 1). The peaks of asbestos, including tremolite and chrysotile, were identified in the samples with 1% and 3% ACMs. In the XRPD profiles, the (002) ($d = 0.730$ nm) and (004) ($d = 0.365$ nm) peaks of chrysotile, which are unique to chrysotile, were observed. However, they were not observed in the samples with 0.1% and 0% ACMs. This means that the peaks of asbestiform tremolite and chrysotile in these samples were weak and broad (Figure 1). They likely overlapped with the main peaks of the matrix materials. These results were homogenous among all the analyzed matrix materials (i.e., talc, vermiculite, and sepiolite). For this reason, additional methods should be used for the detection of trace asbestos in industrial products such as cement, friction materials, and other similar products [1]. The integrated intensities of asbestos peaks for the samples with 1% and 3% ACMs that showed distinguishable peaks were calculated (Tables 1–3). T1–T8, containing 1% asbestos, had integral intensities in the range of 6036–6180, whereas T9–T16, containing 3% asbestos, presented integral intensities in the range of 20,146–21,166 (Table 1). The intensities of T9–T16 were approximately 3.3 times those of T1–T8. The integral intensities of V1–V8, containing 1% asbestos, were in the range of 3006–3422, whereas the integral intensities of V9–V16, containing 3% asbestos, were determined to be in the range of 9408–11,557 (Table 2). The intensities of V9–V16 were approximately 3.4 times those of V1–V8. The integral intensities of S1–S8 and S9–S16 were 9496–11,018 and 20,016–21,910, respectively (Table 3); thus, the latter values were approximately 2.1 times the former. Generally, the intensities of representative peaks in the XRPD profile correlated positively with the concentration of asbestos in matrix materials. Thus, XRPD analysis allows for a quick and simple mineral identification with a detection limit of 1%.

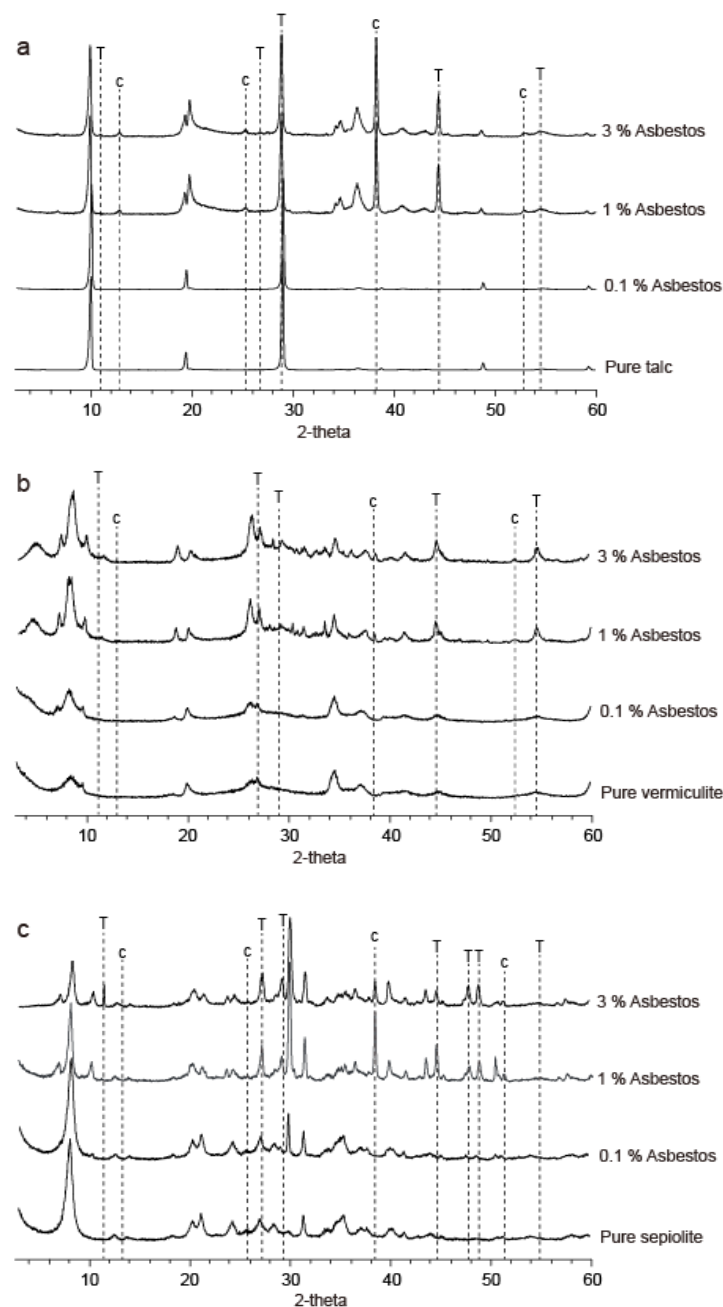


Figure 1. X-ray diffraction patterns of standard asbestos-containing materials (ACMs): (a) talc, (b) vermiculite, and (c) sepiolite with different concentrations of asbestos (0%, 0.1%, 1%, and 3%). T represents asbestiform tremolite; C represents chrysotile.

The critical F value and F ratio of one-way ANOVA were compared to evaluate the homogeneity of the ACM samples. The homogeneity at a 95% confidence level using the p-value was calculated as a statistical value [31]; the analyzed values are summarized in Table 4. The homogeneity of T1–T8, T9–T16, V9–V16, S1–S8, and S9–S16 was evaluated using the statistical test of the one-way ANOVA; the respective F ratios (1.8388, 0.9688, 0.7656, 1.4317, 1.2310) were less than the critical F value (2.6572). This demonstrates homogeneity at a 95% confidence level. However, some F ratios for V1–V8 (3.8964) were higher than the critical F value (2.6572), indicating non-homogeneity at a 95% confidence level. According to these results, three kinds of standard ACMs with various concentrations were sufficiently homogeneous and reproducible [20,32].

Table 1. Integral intensities of asbestos peaks for standard talc samples with different ACM concentrations (1% and 3%).

No.	Integral Intensity			No.	Integral Intensity		
	1	2	3		1	2	3
T1	6266	4789	7236	T9	20,512	17,567	18,319
T2	5399	5385	2458	T10	21,744	16,513	19,647
T3	6874	5860	6624	T11	20,793	21,933	22,993
T4	5828	6230	7330	T12	24,704	21,838	20,618
T5	6845	6257	5552	T13	18,121	21,015	23,730
T6	5828	7410	5714	T14	22,182	18,722	23,055
T7	6136	7013	8095	T15	18,627	23,218	22,257
T8	5565	5346	6427	T16	22,617	20,363	18,707
Avg.	6093	6036	6180	Avg.	21,163	20,146	21,166
SD	549	880	1725	SD	2147	2335	2119

T1–8 contain 1% asbestos, and T9–16 contain 3% asbestos.

Table 2. Integral intensities of asbestos peaks for standard vermiculite samples with different ACM concentrations (1% and 3%).

No.	Integral Intensity			No.	Integral Intensity		
	1	2	3		1	2	3
V1	1976	1140	773	V9	7794	9723	6376
V2	1712	2455	956	V10	15,107	12,506	7065
V3	3303	3702	722	V11	7089	9855	6619
V4	647	2363	915	V12	6373	15122	12880
V5	2487	2384	7027	V13	6775	6729	12584
V6	4540	5355	5896	V14	14,093	7823	11,234
V7	4203	5905	2175	V15	8342	11499	16851
V8	5177	4073	7749	V16	9689	8670	18,849
Avg.	3006	3422	3277	Avg.	9408	10,241	11,557
SD	1566	1636	3068	SD	3376	2715	4713

V1–8 contain 1% asbestos, and V9–16 contain 3% asbestos.

Table 3. Integral intensities of asbestos peaks for standard sepiolite samples with different ACM concentrations (1% and 3%).

No.	Integral Intensity			No.	Integral Intensity		
	1	2	3		1	2	3
S1	7670	9292	10,224	S9	23,627	15,868	23,029
S2	11,133	13,466	12,441	S10	17,171	18,428	22,624
S3	11,132	8976	13,323	S11	20,297	16,305	20,722
S4	7977	11,097	10,260	S12	19,141	21,844	19,389
S5	11,385	11,343	12,337	S13	18,244	22,307	18,799
S6	10,431	9783	9008	S14	22,293	24,458	24,180
S7	9436	6678	11,391	S15	18,188	20,574	22,984
S8	6804	12,749	9156	S16	21,169	22,869	23,549
Avg.	9496	10,423	11,018	Avg.	20,016	20,332	21,910
SD	1800	2197	1600	SD	2235	3150	2007

S1–8 contain 1% asbestos, and S9–16 contain 3% asbestos.

Table 4. Results of the evaluation of sample homogeneity.

Sample No. T1–T8						
Source of Variation	Sum of Squares	Degrees of Freedom	Mean Squares	F Ratio	P-Value	F-Crit
Between groups	12,676,331	7	1,810,904	1.8388	0.1482	2.6572
Among groups	15,757,699	16	984,856			
Total	28,434,030	23				
Sample No. T9–T16						
Source of Variation	Sum of Squares	Degrees of Freedom	Mean Squares	F Ratio	P-Value	F-Crit
Between groups	31,973,313	7	4,597,616	0.9688	0.4854	2.6572
Among groups	75,432,023	16	5,714,501			
Total	107,405,336	23				
Sample No. V1–V8						
Source of Variation	Sum of Squares	Degrees of Freedom	Mean Squares	F Ratio	P-Value	F-Crit
Between groups	64,612,875	7	9230411	3.8964	0.0115	2.6572
Among groups	37,903,497	16	2368969			
Total	102,516,372	23				
Sample No. V9–V16						
Source of Variation	Sum of Squares	Degrees of Freedom	Mean Squares	F Ratio	P-Value	F-Crit
Between groups	76,695,341	7	10,956,477	0.7656	0.6237	2.6572
Among groups	229,000,008	16				
Total	305,695,349	23				
Sample No. S1–S8						
Source of Variation	Sum of Squares	Degrees of Freedom	Mean Squares	F Ratio	P-Value	F-Crit
Between groups	32,276,823	7	4,610,975	1.4317	0.2600	2.6572
Among groups	51,528,728	16	3,220,546			
Total	83,805,551					
Sample No. S9–S16						
Source of Variation	Sum of Squares	Degrees of Freedom	Mean Squares	F Ratio	P-Value	F-Crit
Between groups	52,197,523	7	7,456,360	1.2310	0.3426	2.6572
Among groups	96,916,481	16	6,057,280			
Total	149,114,004	23				

3.2. Electron Microscopy

Scanning and transmission electron microscopy were performed for the samples with 0.1% ACMs (i.e., talc, vermiculite, and sepiolite) to detect the concentration of asbestos (Figures 2 and 3). The SEM imaging revealed that elongate mineral particles were mostly present adjacent to the matrix materials. Most of the elongate mineral particles were over 100 μm in length, and their thickness was not uniform (Figure 2). Elongate mineral particles [33] ranged from 10 to 150 μm in length and from 0.1 to 1 μm in diameter. Chrysotile (Figure 2) was composed of straight, thin, and flexible elongate particles, identifiable as asbestos due to their length/diameter ratio of more than 3 [34,35]. Individual elongate mineral particles presented a rough surface and measured less than 0.1 μm in length, thus being below the SEM resolution [36,37]. The asbestos particles were also observed using TEM. They appeared more isolated than those in the SEM samples (Figure 3), making it easier to find them and

note their morphology in high resolution (Figure 3c). According to a previous study, the detection limit of elongate mineral particles by TEM is approximately 0.01 particles/cm² in the air [1]. This is probably due to the sub-micron size of fine particles that can be observed by TEM (Figure 3) and cannot be detected by XRPD analysis. The peaks of asbestos, including chrysotile and asbestiform tremolite, were very weak and overlapped with the peaks of other minerals. Despite being time-consuming, destructive, and expensive, electron microscopy is essential for the identification and quantification of finer elongate mineral particles in low-concentration ACM samples. As such, electron microscopy should be performed and compared with the XRPD results to improve analytical efficiency. The correlation of a point count method using electron microscopy and the XRPD analysis will be presented in a future study.

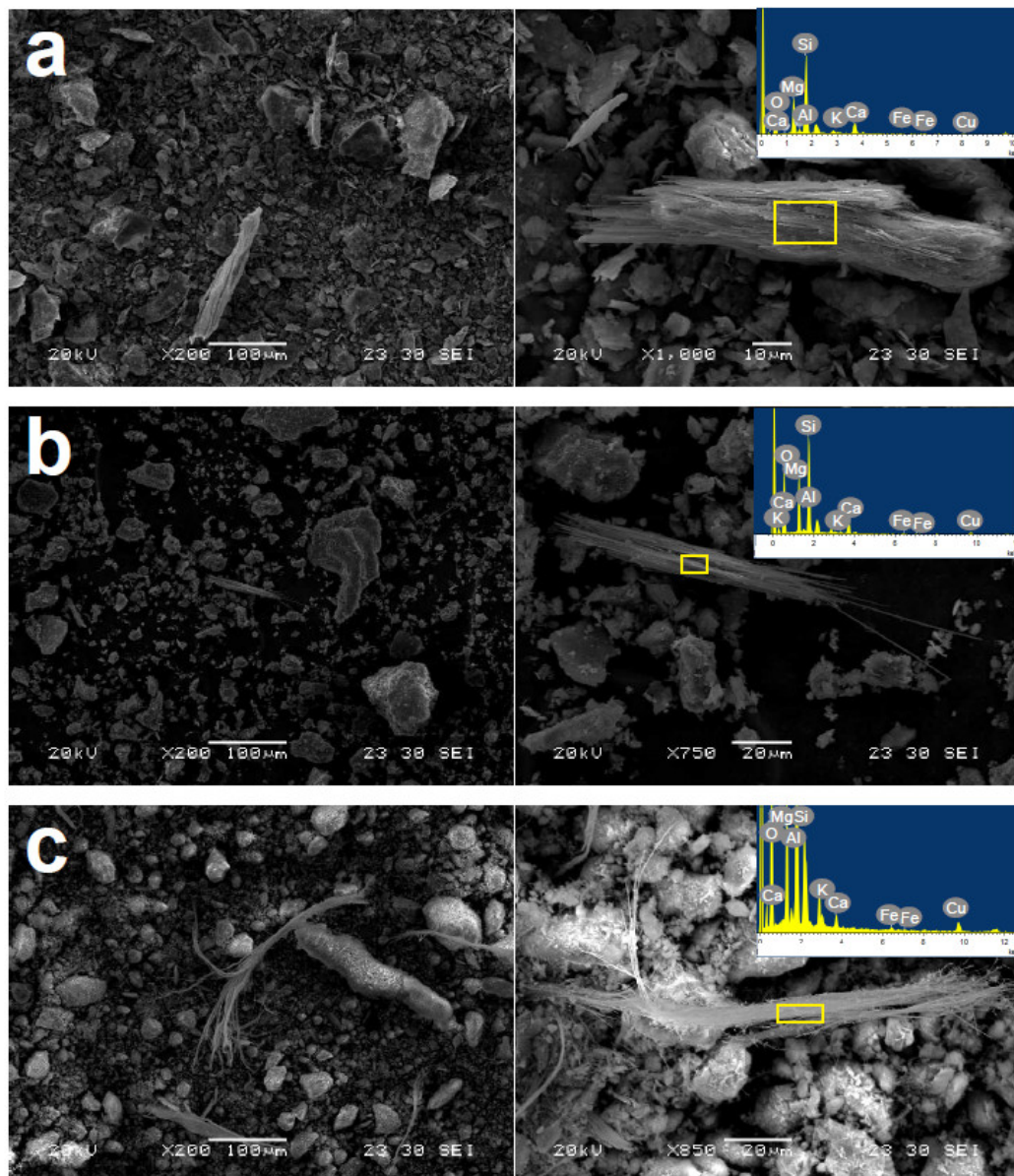


Figure 2. Representative SEM images and EDS spectra of asbestos in a sample with 0.1% ACMs: (a) talc, (b) vermiculite, and (c) sepiolite.

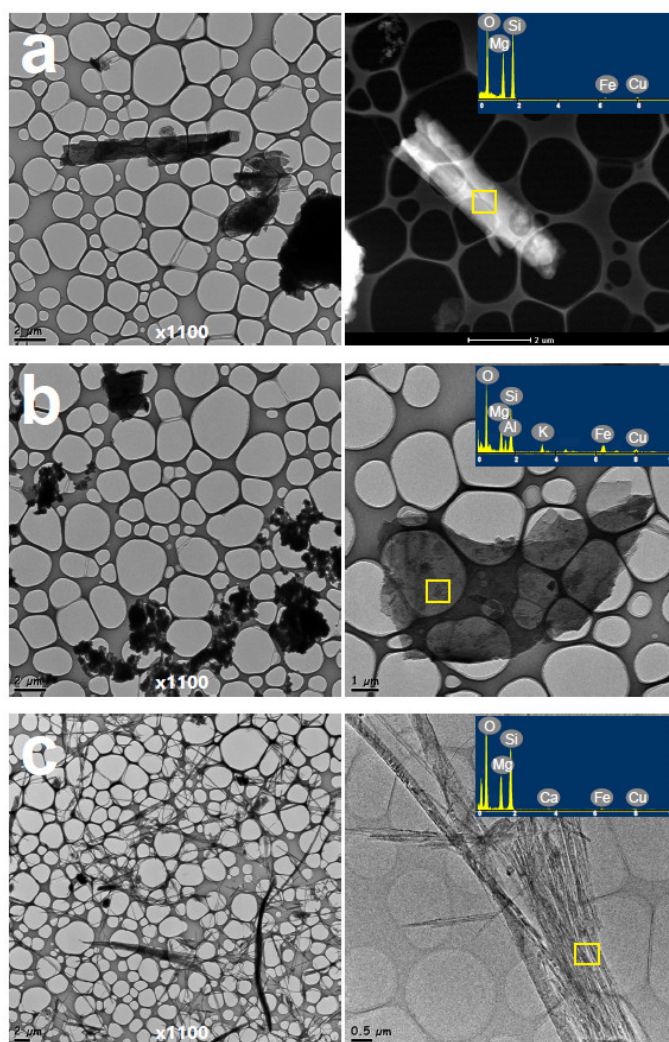


Figure 3. Representative TEM micrographs of asbestos in a sample with 0.1% ACMs: (a) talc, (b) vermiculite, and (c) sepiolite. EDS analysis of the area (inset) further confirms the presence of silicate minerals.

4. Conclusions

This study provides reliable and simple techniques for the identification of trace amounts of asbestos in several matrix materials and suggests a new analytical approach. (a) Various concentrations of ACMs were used for the determination of X-ray diffractometric quantitation. The homogeneity of the standard materials was estimated by the one-way ANOVA test. Our results suggest that standard materials as prepared herein were sufficiently homogenous in mixture phases. The XRPD analysis detected asbestos in the samples with 1% and 3% ACMs; however, the XRPD peak of asbestos was not visible in the samples with 0.1% ACMs. Although the XRPD profiles could be obtained quickly and easily, they presented a detection limit of 1% ACMs. (b) Scanning and transmission electron microscopy allowed for the detection of asbestos in matrix materials with a concentration of 0.1%. The asbestos particles were competently visualized in microscopic images detailing the particle morphology and size. As such, electron microscopy allows for the detection of trace amounts of asbestos and its qualitative estimation, despite being time-consuming, destructive, and expensive.

The analytical efficiency and data reliability can be improved by a combination of X-ray techniques and electron microscopy. The results outlined herein can also be used to detect trace minerals in bulk sediments in natural environments.

Author Contributions: K.Y. designed the study concept and produced the SEM and TEM data. K.-C.Y. revised the manuscript. J.J. contributed to the XRPD data production and manuscript preparation. All authors have read and agreed to the published version of the manuscript.

Funding: This work was funded by a Pusan National University Research Grant, 2020 to K.Y. and an Korea Polar Research Institute (KOPRI) project (PE20180) to K.-C.Y.

Acknowledgments: This work was supported by a Pusan National University Research Grant, 2020 to K.Y. and an Antarctic Project of KOPRI (PE20180) to K.-C.Y.

Conflicts of Interest: The authors declare no conflict of interest.

References

1. Mossman, B.T.; Bignon, J.; Corn, M.; Seaton, A.; Gee, J.B. Asbestos: Scientific developments and implications for public policy. *Science* **1990**, *247*, 294–301. [[CrossRef](#)] [[PubMed](#)]
2. Williams, C.; Dell, L.; Adams, R.; Rose, T.; Van Orden, D. State-of-the-science assessment of non-asbestos amphibole exposure: Is there a cancer risk? *Environ. Geochem. Health* **2013**, *35*, 357–377. [[CrossRef](#)] [[PubMed](#)]
3. Campbell, W.J. *Selected Silicate Minerals and Their Asbestiform Varieties: Mineralogical Definition and Identification-Characterization*; Department of the Interior, Bureau of Mines: Washington, DC, USA, 1977; Volume 8751.
4. Punturo, R.; Ricchiuti, C.; Mengel, K.; Apollaro, C.; De Rosa, R.; Bloise, A. Serpentine-derived soils in southern Italy: Potential for hazardous exposure. *J. Mediterr. Earth Sci.* **2018**, *10*, 51–61.
5. Punturo, R.; Ricchiuti, C.; Bloise, A. Assessment of Serpentine Group Minerals in Soils: A Case Study from the Village of San Severino Lucano (Basilicata, Southern Italy). *Fibers* **2019**, *7*, 18. [[CrossRef](#)]
6. Kim, H.-W.; Park, G.-Y.; Han, J.-G.; Han, Y.-S.; Hwang, B.-G.; Lee, J.-H. Releasing of asbestos fibers from the weathered asbestos cement slate roofing. *J. Korean Soc. Occup. Environ. Hyg.* **2010**, *20*, 88–93.
7. Murr, L.E.; Soto, K. TEM comparison of chrysotile (asbestos) nanotubes and carbon nanotubes. *J. Mater. Sci.* **2004**, *39*, 4941–4947. [[CrossRef](#)]
8. Wagner, J.C.; Sleggs, C.A.; Marchand, P. Diffuse pleural mesothelioma and asbestos exposure in the North Western Cape Province. *Occup. Environ. Med.* **1960**, *17*, 260–271. [[CrossRef](#)]
9. World Health Organization. Asbestos and other natural mineral fibres. International programme on chemical safety. *Environ. Health Criteria* **1986**, *53*, 194.
10. Skinner, H.C.W.; Ross, M.; Frondel, C. *Asbestos and Other Fibrous Materials: Mineralogy, Crystal Chemistry, and Health Effects*; Oxford University Press: Oxford, UK, 1988.
11. Mossman, B.T.; Gee, J.B.L. Asbestos-related diseases. *New Engl. J. Med.* **1989**, *320*, 1721–1730. [[CrossRef](#)]
12. Jablonski, R.P.; Kim, S.; Cheres, P.; Liu, G.; Kamp, D.W. Insights into mineral fibre-induced lung epithelial cell toxicity and pulmonary fibrosis. In *Mineral Fibres: Crystal Chemistry, Chemical-Physical Properties, Biological Interaction and Toxicity*; Northwestern University: Evanston, IL, USA, 2017; pp. 447–500.
13. WHO. *Guidelines for Drinking-Water Quality*; World Health Organization: Geneva, Switzerland, 2004; Volume 1.
14. Becklake, M.R. Asbestos-related diseases of the lung and other organs: Their epidemiology and implications for clinical practice. *Am. Rev. Respir. Dis.* **1976**, *114*, 187–227.
15. International Agency for Research on Cancer. Asbestos (chrysotile, amosite, crocidolite, tremolite, actinolite, and anthophyllite). In *Metals, Arsenic, Dusts and Fibres; A review of human carcinogens*; World Health Organization: Geneva, Switzerland, 2012; pp. 219–309.
16. Samet, J.M.; Dominici, F.; Curriero, F.C.; Coursac, I.; Zeger, S.L. Fine particulate air pollution and mortality in 20 US cities, 1987–1994. *New Engl. J. Med.* **2000**, *343*, 1742–1749. [[CrossRef](#)] [[PubMed](#)]
17. Europe, W. *Air Quality Guidelines*, 2nd ed.; Regional Office for Europe: Copenhagen, Denmark, 2000.
18. LaDou, J.; Castleman, B.; Frank, A.; Gochfeld, M.; Greenberg, M.; Huff, J.; Joshi, T.K.; Landrigan, P.J.; Lemen, R.; Myers, J. The case for a global ban on asbestos. *Environ. Health Perspect.* **2010**, *118*, 897–901. [[CrossRef](#)] [[PubMed](#)]
19. Della Ventura, G.; Vigliaturo, R.; Gieré, R.; Pollastri, S.; Gualtieri, A.F.; Iezzi, G. Infra Red Spectroscopy of the Regulated Asbestos Amphiboles. *Minerals* **2018**, *8*, 413. [[CrossRef](#)] [[PubMed](#)]

20. Asahi, T.; Kobayashi, S.; Nakayama, K.; Konya, T.; Fujinawa, G.; Nakamura, T. Preparation and evaluation of a chrysotile asbestos-containing standard material for validating x-ray diffractometric quantitation. *Anal. Sci.* **2011**, *27*, 1217. [[CrossRef](#)] [[PubMed](#)]
21. Wang, N.; Jaurand, M.; Magne, L.; Kheuang, L.; Pinchon, M.; Bignon, J. The interactions between asbestos fibers and metaphase chromosomes of rat pleural mesothelial cells in culture. A scanning and transmission electron microscopic study. *Am. J. Pathol.* **1987**, *126*, 343.
22. Bloise, A.; Miriello, D. Multi-analytical approach for identifying asbestos minerals in situ. *Geosciences* **2018**, *8*, 133. [[CrossRef](#)]
23. Januch, J.; Brattin, W.; Woodbury, L.; Berry, D. Evaluation of a fluidized bed asbestos segregator preparation method for the analysis of low-levels of asbestos in soil and other solid media. *Anal. Methods* **2013**, *5*, 1658–1668. [[CrossRef](#)]
24. Borchert, H.; Shevchenko, E.V.; Robert, A.; Mekis, I.; Kornowski, A.; Grübel, G.; Weller, H. Determination of nanocrystal sizes: A comparison of TEM, SAXS, and XRD studies of highly monodisperse CoPt₃ particles. *Langmuir* **2005**, *21*, 1931–1936. [[CrossRef](#)]
25. Compton, S.P. TEM Quantification of Amphibole in Asbestos Containing Materials: A Summary of Data 20 Years in the Making. *Microsc. Microanal.* **2018**, *24*, 1184–1185. [[CrossRef](#)]
26. Vigliaturo, R.; Pollastri, S.; Gieré, R.; Gualtieri, A.F.; Dražić, G. Experimental quantification of the Fe-valence state at amosite-asbestos boundaries using acSTEM dual-electron energy-loss spectroscopy. *Am. Mineral.* **2019**, *104*, 1820–1828. [[CrossRef](#)]
27. Engelmann, H.-J. Advantages and Disadvantages of TEM Sample Preparation Using the FIB Technique. *Prakt. Metallogr.* **2003**, *40*, 163–174.
28. Vigliaturo, R.; Della Ventura, G.; Choi, J.K.; Marengo, A.; Lucci, F.; O’Shea, M.J.; Pérez-Rodríguez, I.; Gieré, R. Mineralogical characterization and dissolution experiments in Gamble’s solution of Tremolitic amphibole from Passo di Caldenno (Sondrio, Italy). *Minerals* **2018**, *8*, 557. [[CrossRef](#)] [[PubMed](#)]
29. Gualtieri, A.F. Naturally Occurring Asbestos: A Global Health Concern? State of the Art and Open Issues. *Environ. Eng. Geosci.* **2020**, *26*, 3–8. [[CrossRef](#)]
30. Hirsch, R.F. Analysis of variance in analytical chemistry. *Anal. Chem.* **1977**, *49*, 691A–700A. [[CrossRef](#)]
31. Guide, I. *General Requirements for the Competence of Reference Material Producers*; ISO: Geneva, Switzerland, 2009.
32. Guide, I. *35 Reference Materials—General and Statistical Principles for Certification*; International Organization for Standardization: Geneva, Switzerland, 2006.
33. Schulte, P.S.; Trout, D.; Zumwalde, R.D. *Asbestos Fibers and Other Elongate Mineral Particles: State of the Science and Roadmap for Research*; United States Department of Health and Human Services: Washington, DC, USA, 2011.
34. Davis, J.M. *In Vivo Assays to Evaluate the Pathogenic Effects of Minerals in Rodents*; Mineralogical Society of America: Washington, DC, USA, 1993.
35. Militello, G.M.; Sanguineti, E.; Yus González, A.; Mantovani, F.; Gaggero, L. The Concentration of Asbestos Fibers in Bulk Samples and Its Variation with Grain Size. *Minerals* **2019**, *9*, 539. [[CrossRef](#)]
36. Yang, H.; Xiao, Y.; Liu, K.; Yang, Y.; Feng, Q. Physicochemical dispersion of chrysotile. *Colloids Surf. A Physicochem. Eng. Asp.* **2007**, *301*, 341–345. [[CrossRef](#)]
37. Bloise, A.; Ricchiuti, C.; Lanzafame, G.; Punturo, R. X-ray synchrotron microtomography: A new technique for characterizing chrysotile asbestos. *Sci. Total Environ.* **2020**, *703*, 135675. [[CrossRef](#)]

